Bull. Mater. Sci. (2020) 43:15
https://doi.org/10.1007/s12034-019-1989-8

Investigating the role of amides on the textural and optical properties of mesoporous-nanostructured θ-Al_2O_3

SOURAV GHOSH[1,2], SUKANYA KUNDU[1,3], RITUPARNA DAS[1] and MILAN KANTI NASKAR[1,3,*]
[1]Sol–Gel Division, CSIR-Central Glass and Ceramic Research Institute, Kolkata 700032, India
[2]Department of Chemical Sciences, Indian Institute of Science Education and Research (IISER) Kolkata, Mohanpur 741246, India
[3]Academy of Scientific and Innovative Research (AcSIR), Ghaziabad 201002, India
*Author for correspondence (milan@cgcri.res.in)

MS received 21 May 2019; accepted 26 July 2019

Abstract. Mesoporous-nanostructured θ-Al_2O_3 was synthesized by an autoclaving technique using different amides i.e., formamide (F), dimethyl formamide (DMF) and diethyl formamide (DEF) at 150°C/24 h followed by calcination at 1000°C. Crystallization and structural behaviour of the as-synthesized materials were characterized by X-ray diffraction and Fourier transform infrared spectroscopy. The porosity study was carried out by N_2 adsorption–desorption (BET) technique. Microstructural features were measured by transmission electron microscopy (TEM). The amide-based solvents played a deliberate role in microstructural and textural features of θ-Al_2O_3. The DMF-based solvent showed an enhanced surface area of 158 $m^2\,g^{-1}$. The as-prepared θ-Al_2O_3 rendered a nano-sheet, nano-rod and nano-flake like morphology for F, DMF and DEF derived products, respectively. From the UV–Vis spectroscopic measurement, the estimated band-gap of θ-Al_2O_3 was found to be 5.16–5.40 eV. Photoluminescence investigation further revealed blue emission particularly for excitation at a wavelength of 252 nm. A DMF-derived sample rendered the lowest band gap due to its smaller crystallite size and higher surface area compared to that of F- and DEF-derived samples.

Keywords. θ-alumina; autoclaving technique; mesoporosity; microstructure; photoluminescence.

1. Introduction

Fabrication of mesoporous alumina with controllable architecture is primarily essential for its extensive application arena in ceramics, sensing, membranes, adsorption, catalysis and catalytic supports [1–6]. The potency of alumina nanostructure indeed depends on its textural and structural frameworks. Theta alumina (θ-Al_2O_3), in particular is known as a good candidate for optical photoluminescence (PL) applications [7]. Among all alumina polymorphs, θ-Al_2O_3 is structurally unique due to its equal distribution of aluminium cations (Al^{+3}) among tetrahedral and octahedral lattice positions within an oxide framework [8]. Instead of metastability, θ-Al_2O_3 is a stable framework with monoclinic symmetry. A larger crystallite size and fewer numbers of defects in the crystalline framework further facilitate its tunable optical applications. However, fabrication of pure θ-Al_2O_3 nanostructures is relatively tricky and rarely explored in the literature. Gangwar *et al* [9] successfully synthesized θ-Al_2O_3 nanowires particularly for rapid optical sensing application. Stability of θ-Al_2O_3 was determined by introducing a catalytic amount of chromium (Cr), which was further theoretically explained by Lodziana *et al* [10]. The luminescence feature of such alumina nanostructures is admirable due to their complex lattice dynamics, high thermal sustainability and ideal electronic band alignment. This encourages us to fabricate mesoporous θ-Al_2O_3 nanostructures by a cost-effective template-free method specifically for textural and optical investigations.

Herein, we have reported a facile synthetic strategy to design mesoporous θ-Al_2O_3 nanostructures using different amide-based solvents, ABS (formamide (F), dimethyl formamide (DMF) and diethyl formamide (DEF)). Employment of ABS contributed a significant *in-situ* structure directing and pore-templating effects towards the crystalline framework of θ-Al_2O_3. In this report, the influence of ABS (F, DMF and DEF) on the preparation of θ-Al_2O_3 has been illustrated in terms of its textural, morphological and optical properties. An extensive correlation among nanostructures, textural features and optical properties has been established.

Electronic supplementary material: The online version of this article (https://doi.org/10.1007/s12034-019-1989-8) contains supplementary material, which is available to authorized users.

Published online: 18 December 2019

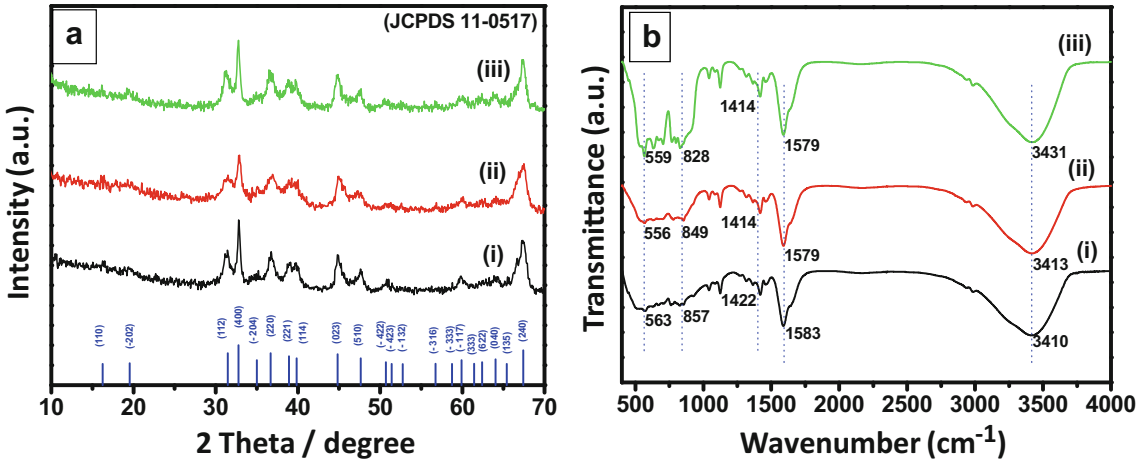

Figure 1. (**a**) XRD and (**b**) FTIR patterns of θ-Al_2O_3 derived from (i) F, (ii) DMF and (iii) DEF.

2. Materials and method

2.1 *Materials preparation*

All the chemicals were analytical grade and employed without any purification.

For the preparation of θ-Al_2O_3, 5 mmol $Al(NO_3)_3{\cdot}9H_2O$ was added into 5 ml of Millipore water followed by addition of 100 mmol of F, DMF and DEF each under stirring conditions. The homogeneous solution was treated by an autoclaving technique at 150°C/24 h. After completion of the reaction, the as-prepared sample was centrifuged and washed. Then the wet product was dried at 60°C in an oven for 12 h. The dried powder was heated at 500°C/1 h with a heating rate of 1°C min^{-1} followed by rising temperature up to 1000°C/1 h with a heating rate of 5°C min^{-1}.

2.2 *Characterization*

The phase-investigation was performed by powder X-ray diffractometer (PXRD, Philips X'Pert Pro PW 3050/60, 40 kV and 30 mA) with Cu-Kα (wavelength of 0.15418 nm) and nickel filter setup for phase purity. The d (crystallite size) value of θ-Al_2O_3 powder was measured by Scherrer's mathematical relation: $d = 0.9\lambda/B \cos\theta$, where, λ, B and θ are the wavelength of Cu-Kα (0.154 nm), full width at half maximum of the highest intense PXRD peak (radian) and the angle of the corresponding peak, respectively. Structural characterization was further carried out by Fourier transform infrared (FTIR) spectroscopy (Nicolet 5PC, Madison, WI, KBr pellet) with a resolution of 4 cm^{-1}. The surface area and porosity were measured by a nitrogen adsorption–desorption technique (ASIQ MP, Quantachrome) with a degassing temperature of 250°C for 4 h. The Brunauer–Emmett–Teller (BET) and Barrett–Joyner–Halenda (BJH) methods were used to analyse the surface area and pore size distribution of the samples, respectively. The pore volume was calculated from a nitrogen adsorption volume at (p/p_0) of 0.99. Microstructural feature of θ-Al_2O_3 was investigated by transmission electron microscopy (TEM, 300 kV, Tecnai G2 30ST). The optical property of samples was examined by a UV–VIS–NIR spectrophotometer (UV3600, Shimadzu, Japan). PL studies were recorded by using a Horiba Jobin Yvon Fluoromax 4 spectrophotometer equipped with a 150 W Xe lamp.

3. Results and discussion

3.1 *Structural studies*

The crystallization study of the sample is shown by the PXRD pattern of the 1000°C calcined sample using F and its derivatives such as DMF and DEF (figure 1a). The crystalline peaks resembled with the formation of θ-Al_2O_3 (JCPDS 11-0517). The diffraction patterns of possible other alumina polymorphs could not be obtained during PXRD measurement indicating phase pure θ-Al_2O_3. The crystallite size of θ-Al_2O_3 was within the range of 7.6–8.5 nm. It is observed that there are no adequate changes in the crystal phase with the variation of ABS (F, DMF and DEF). However, calcination at relatively low temperature (800°C) rendered the formation of γ-Al_2O_3 (supplementary figure S1, ESI). Therefore, high-calcination temperature was required for the phase transformation from γ-Al_2O_3 to θ-Al_2O_3.

Figure 1b presents FTIR spectra of θ-Al_2O_3 prepared using different ABS (F, DMF and DEF). For θ-Al_2O_3, Al–O stretching vibration mode of the tetrahedral coordination unit (AlO_4) was identified from vibration modes at around 750–850 cm^{-1}, while 550–600 cm^{-1} was originated from an octahedral unit. The appearance of peaks at ∼1580 and ∼3400 cm^{-1} corresponds to the bending and stretching modes of the intercalated hydroxyl group, respectively [11]. It is pointed out that with

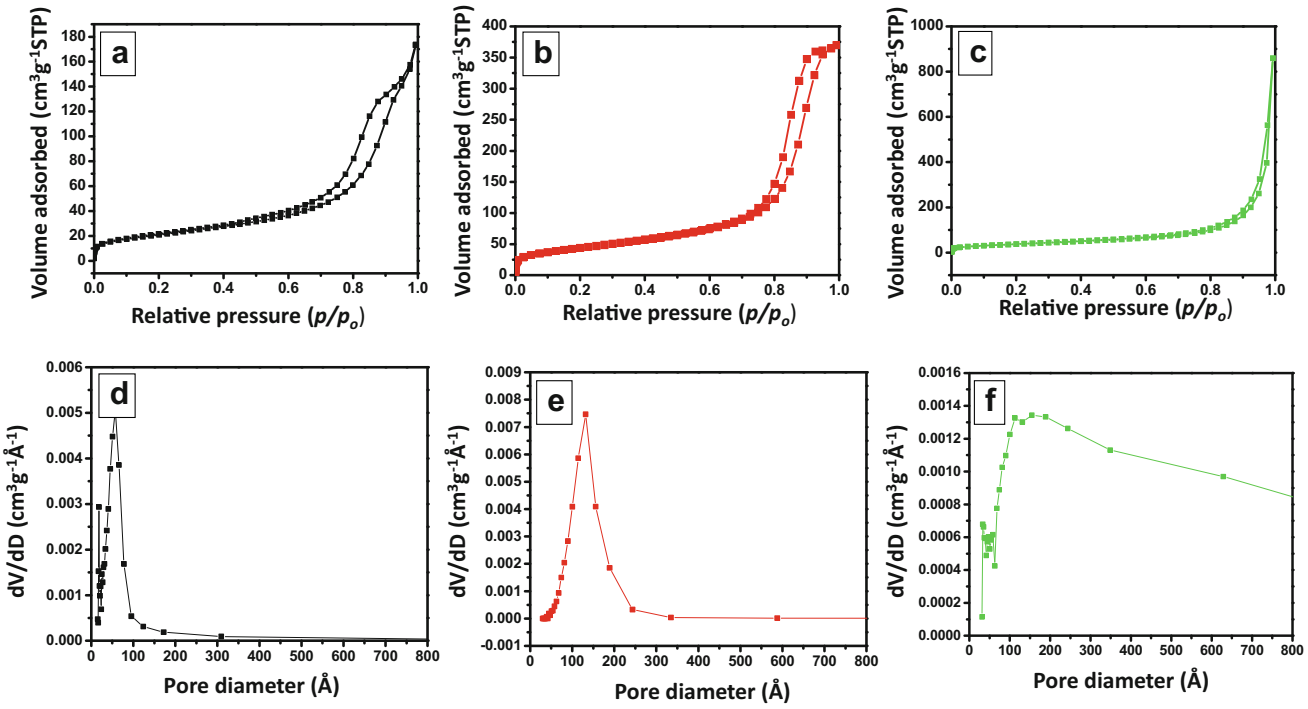

Figure 2. (**a–c**) Nitrogen adsorption–desorption isotherms and (**d–f**) pore size distributions of θ-Al_2O_3 derived from (**a**, **d**) F, (**b**, **e**) DMF and (**c**, **f**) DEF.

Table 1. Textural properties of θ-Al_2O_3 (calcined at 1000°C) obtained from different ABS.

Sample ID[a]	Crystallite size (nm)	S_{BET} ($m^2\ g^{-1}$)[b]	V_p ($cm^3\ g^{-1}$)[c]	D (nm)[d]
F/24/20	8.4	76	0.26	7.03
DMF/24/20	7.6	158	0.57	14.53
DEF/24/20	8.1	137	1.33	38.8

[a]Solvent/time (h)/mol of ABS per mol of Al(III).
[b]BET surface area.
[c]Total pore volume.
[d]Average pore diameter.

variation of ABS (F, DMF and DEF), no remarkable changes were noticed.

Figure 2 shows the nitrogen adsorption–desorption isotherm (a–c) and pore-size distribution (d–f) of the synthesized θ-Al_2O_3 samples. It demonstrates type IV isotherm (according to IUPAC classification) indicating mesoporosity of samples [12]. It is worth mentioning that variation of ABS directly influences hysteresis loops in isotherm. The F-derived sample shows a H4 type curve with a narrow slit-like pore geometry as revealed by a near-horizontal plateau at lower p/p_0. The nature of isotherm is further changed into H2 type in the presence of DMF indicating ink-bottle pore and/or pore constrictions [13]. For the DEF-derived product, interconnected slit-like pore geometry is observed indicating a H3 type hysteresis loop. Table 1 shows the pore volume, pore diameter, BET surface area and crystallite size values of different ABS-derived samples. The BET surface area values for F-, DMF- and DEF-derived products were found to be 76, 158 and 137 $m^2\ g^{-1}$, respectively. A significant changes in the pore diameter and pore volume occurred among different ABS-derived products. The pore-size distribution was broader for the θ-Al_2O_3 sample due to the existence of irregular interparticle voids at high-calcination temperature. The textural property of the θ-Al_2O_3 (calcined at 1000°C) sample was compared with γ-Al_2O_3 (calcined at 800°C). Supplementary figure S2 (ESI) shows nitrogen adsorption–desorption isotherm and pore-size distribution of the synthesized γ-Al_2O_3 sample. The textural features of γ-Al_2O_3 are represented in supplementary table S1 (ESI). It further revealed the significant increment of the

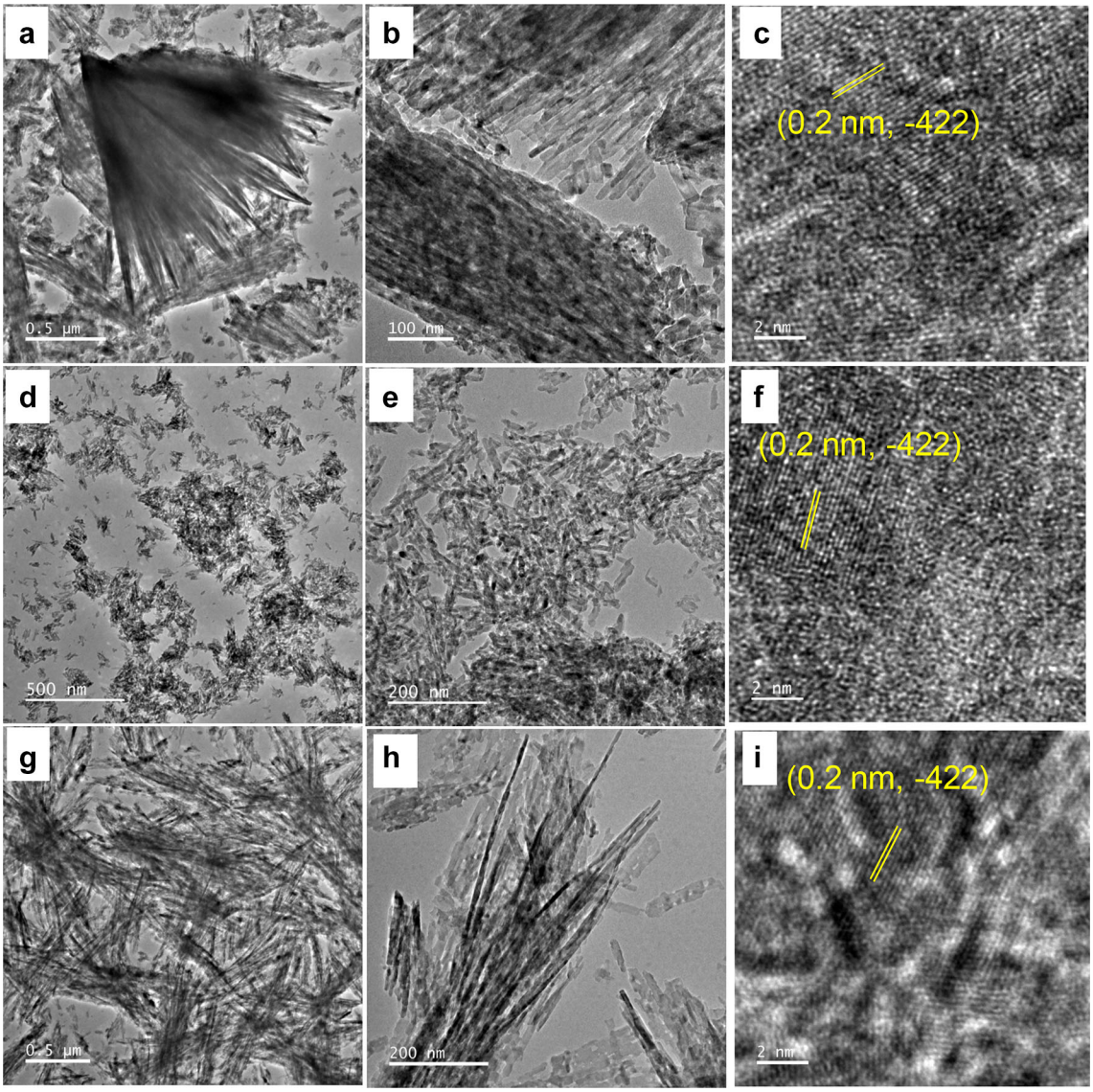

Figure 3. TEM images of θ-Al_2O_3 derived from (**a–c**) F, (**d–f**) DMF and (**g–i**) DEF.

pore-size for the DMF and DEF assisted sample from 800 to 1000°C. The reduction of the surface area and increment of the pore size were attributed to coalescence of mesoporosity with an increase in the calcination temperature. This phenomenon could be attributed to pore swelling and templating properties of the hydrolysis products of ABS. During hydrolysis ABS releases ammonia (NH_3), dimethyl amine ($HNMe_2$) and diethyl amine ($HNEt_2$) along with formic acid (HCOOH) from F, DMF and DEF, respectively [14]. It is interesting to reveal that hydrophobicity of the hydrolysed product increases as $NH_3 < HNMe_2 < HNEt_2$, which further assists the pore swelling to enhance the pore diameter and pore volume within the θ-Al_2O_3 sample [15]. The lower crystallite size further enlarges the surface area for the DMF assisted sample as compared to F- and DEF-derived products.

Figure 3 shows the TEM images of θ-Al_2O_3 prepared using (a–c) F, (d–f) DMF and (g–i) DEF. For the F-derived sample, a nano-sheet-like architecture was obtained along with plenty of interparticle voids. However, nano-rods and nano-sheet-shaped nanostructures were formed in the presence of DMF and DEF, respectively. Microstructural analysis further depicts nanorods having an aspect ratio of 8–30 for the DMF-derived sample, while elongated nano-flakes appeared for the DEF modified sample (aspect ratio of ∼800). However, close inspection of the samples reveals the existence of plenty of elongated nano-flakes which are further self-assembled together to form nano-sheets (supplementary figure S3, ESI). The microstructural variation in the presence of different ABS (F, DMF and DEF) is governed by the sticking and scrolling mechanism with a dissolution–recrystallization process [16]. During the autoclaving treatment, pH of the solution was

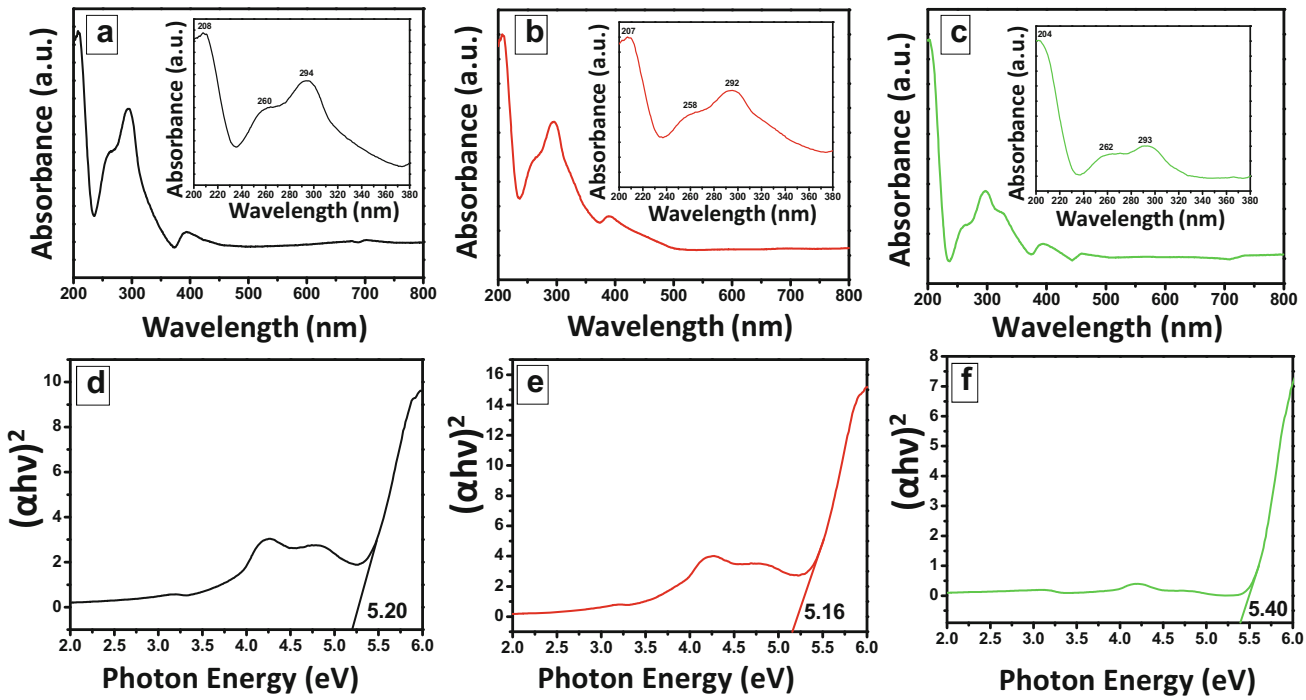

Figure 4. (**a**–**c**) UV–Vis absorption spectra and (**d**–**f**) $(\alpha h\nu)^2$ *vs.* photon energy plot of θ-Al_2O_3 derived from (**a**, **d**) F, (**b**, **e**) DMF and (**c**, **f**) DEF.

acidic for the amide-derived sample (pH 4 to 5.5). In acidic medium, the layer structure of boehmite was disrupted due to the presence of excess protons in solution. Bell *et al* [17] further demonstrated the formation of γ-Al_2O_3 through the scrolling mechanism of the disrupted boehmite layer (2D) into the corresponding favourable microstructure to reduce the surface energy under acidic conditions. Again, intercalation of the *in-situ* hydrolysed product redirected the morphology of the sample through the dissolution–recrystallization process [18,19]. The polycrystalline features of θ-Al_2O_3 were further confirmed by high-resolution transmission electron microscopy analysis. It also demonstrates the inter-planner spacing of 0.2 nm corresponding for the (−422) plane of θ-Al_2O_3. It is worth mentioning that hydrolysis products (NH_3, $(CH_3)_2NH$ and $(C_2H_5)_2NH$) of amides play a deliberate role in porous architecture *via* several kinds of weak electrostatic interactions and entropic involvement of the hydrophobic moiety [19].

3.2 *Optical studies*

An optical property of the sample has been investigated by UV–Vis diffuse reflectance measurement. Figure 4 presents the UV–Vis diffuse reflectance spectra (a–c) and the band-gap energy plot (d–f) of θ-Al_2O_3 obtained from (a, d) F, (b, e) DMF and (c, f) DEF. For further clarity, a high-resolution UV–Vis diffuse reflectance pattern is shown in the insets of figure 4. In UV–Vis diffuse reflectance spectra, three absorption bands were obtained at ∼208 nm (5.96 eV), ∼258 nm (4.80 eV) and ∼292 nm (4.24 eV). The major absorption peak at ∼208 nm (5.96 eV) is originated because of charge transfer $O^{2-} \rightarrow Al^{3+}$, while other two absorption peaks are due to different absorption sites of the θ-Al_2O_3 framework [8,9]. The band-gap is measured from optical UV–Vis spectra from Tauc mathematical relation:

$$(\alpha h\nu)^{1/n} = A(h\nu - E_g)$$

where α, h, $h\nu$, A and E_g represent the absorption coefficient, Planck's constant, photon energy, proportionality constant and optical band gap of the sample, respectively. The band gap is calculated by extrapolating the linear region considering direct transition ($n = 1/2$) from the plot of $(\alpha h\nu)^2$ *vs.* $h\nu$. The optical band gap values were obtained as 5.2, 5.16 and 5.4 eV for F-, DMF- and DEF-derived θ-Al_2O_3, respectively [20]. Accumulation of surface atoms within the nano-scale regime is actually depending on the particle size and morphological feature of samples. A particle with a smaller crystallite size and higher surface area reinforces higher surface pressure as well as higher lattice strain, which could be reason behind the lowest band-gap value for the DMF-derived sample [21]. However, Mondal *et al* [22] recently demonstrated the lower band gap energy of CdS nanorod architecture in comparison with nanoclusters and nanoparticles on the basis of increasing strain of the crystallite. Therefore, the lowest band gap value for the DMF-derived sample could be due to the smaller crystallite size

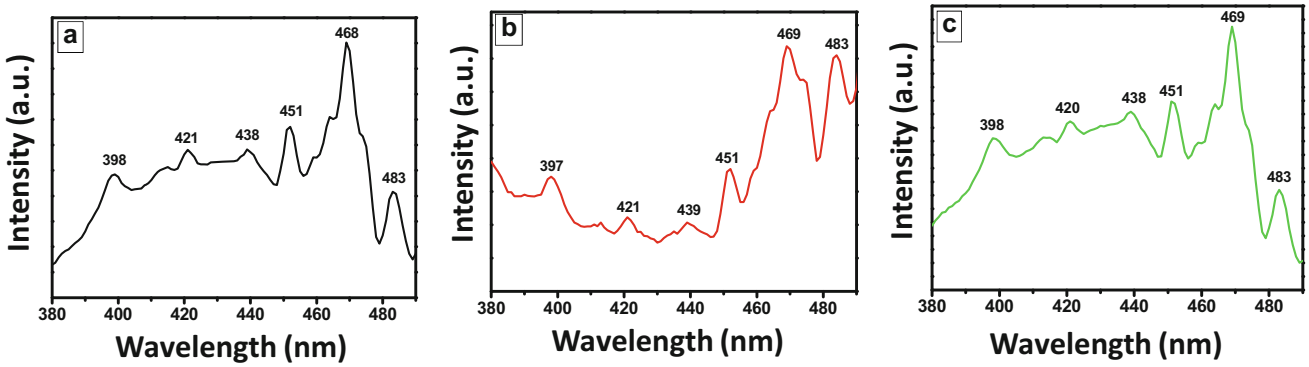

Figure 5. PL spectra of θ-Al_2O_3 derived from (**a**) F, (**b**) DMF and (**c**) DEF.

and higher surface area (S_{BET}) value as well as nanorod-like architecture compared to that of F- and DEF-derived samples.

The enhanced optical property of the sample is further analysed by PL spectra of F, DMF and DEF modified θ-Al_2O_3 (figure 5). In the luminescence spectrum, a broad emission spectrum at around 380–520 nm (2.38–3.26 eV) was obtained at an excitation wavelength of 252 nm (4.91 eV). The appearance of the major two broad peaks at around 397 and 421 nm (3.12 and 2.94 eV) corresponds to the blue emission of the sample. The existence of cationic vacancy of Al^{+3} as well as the F^+-centre could be the reason behind intense blue emission at around 397 nm [23]. However, intense emission at around 421 nm could be originated from the F-centre [24]. Further, spectrum analysis exhibited the presence of one blue emission of the sharp peak at around 469 nm (2.64 eV) together with weak shoulder peaks of blue emission at around 439, 451 and 483 nm (2.82, 2.74 and 2.56 eV). Appearance of such weak shoulder peaks could be due to F_2 centres [25]. It is important to mention that hydrolysis products (NH_3, $(CH_3)_2NH$ and $(C_2H_5)_2NH$) of amides have a key role as the structure directing agent, which further influence the optical absorption spectrum as well as the band gap of the θ-Al_2O_3 sample.

4. Conclusions

Mesoporous θ-Al_2O_3 with a tunable nanostructure was synthesized using different ABS (F, DMF and DEF) under autoclaving conditions at 150°C/24 h followed by calcination at 1000°C. DMF assisted θ-Al_2O_3 rendered the highest surface area of 158 $m^2\,g^{-1}$. The high-surface area and pore size of θ-Al_2O_3 are attributed to templating and structure directing property of NH_3, $(CH_3)_2NH$ and $(CH_3CH_2)_2NH$ obtained from hydrolysis of F, DMF and DEF, respectively. Controllable architecture along with large abundance of mesoporosity enhanced optical property through lowering the band gap value. It demonstrated blue emission, particularly for excitation at a wavelength of 252 nm. The lowest band gap value for the DMF-derived sample could be due to the smaller crystallite size and higher S_{BET} value compared to that of F- and DEF-derived samples. This investigation could be convincing for the fabrication of mesoporous ceramics even at high temperature, particularly for membrane and refractory technological arena.

Acknowledgements

RD is thankful to UGC and SG is thankful to DST-SERB for providing National Postdoctoral Fellowship with project no. PDF/2017/001728. SK is thankful to Academy of Scientific and Innovative Research (AcSIR).

References

[1] Misra C 1986 *ACS Monogr. Ser.* **184** 133
[2] Cortright R D, Davda R R and Dumesic J A 2002 *Nature* **418** 964
[3] Argo A M, Odzak J F, Lai F S and Gates B C 2002 *Nature* **415** 623
[4] Saha D and Das S 2018 *Trans. Indian Ceram. Soc.* **77** 138
[5] Shen S, Ng W K, Chia L S O, Dong Y C and Tan R B H 2012 *Cryst. Growth Des.* **12** 4987
[6] Yang F, Wang Q, Yan J, Fang J, Zhao J and Shen W 2012 *Ind. Eng. Chem. Res.* **51** 15386
[7] Mo S D and Ching W Y 1998 *Phys. Rev. B: Condens. Matter.* **57** 15219
[8] Gangwar J, Gupta B K, Tripathi S K and Srivastava A K 2015 *Nanoscale* **7** 13313
[9] Gangwar J, Gupta B K, Kumar P, Tripathi S K and Srivastava A K 2014 *Dalton Trans.* **43** 17034
[10] Lodziana Z, Topsoe N Y and Norskov J K 2004 *Nat. Mater.* **3** 289
[11] Ghosh S, Roy M and Naskar M K 2014 *Cryst. Growth Des.* **14** 2977
[12] Ghosh S and Naskar M K 2013 *J. Am. Ceram. Soc.* **96** 1698
[13] Sangwichien C, Aranovich G L and Donohue M D 2002 *Colloids Surf. A* **206** 313
[14] Borrows A D, Cassar K, Friend R M W, Mahon M F, Rigby S P and Warren J E 2005 *CrystEngComm* **7** 548

[15] Rekker R 1979 *Eur. J. Med. Chem.* **14** 479
[16] Yang Q 2010 *Inorg. Mater.* **46** 953
[17] Bell T E, Gonzaalez-Carballo J M, Tooze R P and Torrente-Murciano L 2015 *J. Mater. Chem. A* **3** 6196
[18] Ghosh S, Das R and Naskar M K 2016 *J. Am. Ceram. Soc.* **99** 2273
[19] Lupulescu A I, Kumar M and Rimer J D 2013 *J. Am. Chem. Soc.* **135** 6608
[20] Lee C K, Cho E, Lee H S, Seol K S and Han S 2007 *Phys. Rev. B: Condens. Matter.* **76** 245110
[21] Deotale A J and Nandedkar R V 2016 *Mater. Today: Proc.* **3** 2069
[22] Mondal S, Sudhu S, Bhattacharya S and Saha S K 2015 *J. Phys. Chem. C* **119** 27749
[23] Yu Z Q, Chang D, Li C, Zhang N, Feng Y Y and Dai Y Y 2001 *J. Mater. Res.* **16** 1890
[24] Chang C C, Wu J L, Yang N H, Lin S J and Chang S Y 2012 *CrystEngComm* **14** 1117
[25] Toshima R, Miyamaru H, Asahara J, Murasawa T and Takahashi A 2002 *J. Nucl. Sci. Technol.* **39** 15